A Family of Class EF Resonant Inverters With Constant AC Voltage Output and Load-Independent Characteristics

Yi Cheng, *Student Member, IEEE*, Yueshi Guan, *Senior Member, IEEE*, Tingting Yao, *Member, IEEE*, Jiachao Zong, *Student Member, IEEE*, Yijie Wang, *Senior Member, IEEE*, and Dianguo Xu, *Fellow, IEEE*

***Abstract*—A family of Class EF resonant inverters with constant ac voltage output and load-independent characteristics is proposed in this article. Moreover, the design principle of Class EF resonant topologies and their load-independent characteristics are concluded. The low voltage or current stress across the switch can be achieved by the second-order resonant network. Furthermore, the common-ground Class E/F resonant inverter and its load-independent design procedure are introduced. Constant ac voltage output and zero-voltage switching can be achieved by the proposed inverter for a wide load range. To validate the theoretical analysis, the 1-MHz experimental prototype is built and the peak efficiency is 93.4%.**

***Index Terms*—Class EF, constant ac voltage output, load-independent, zero-voltage switching (ZVS).**

I. Introduction

HIGH-FREQUENCY resonant inverters are widely applied in wireless power transfer, plasma acceleration, gate driver, etc. [1], [2], [3], [4]. As the operating frequency increases to the multi-MHz range, high-frequency resonant topologies with soft switching characteristics, such as Class E, Class E/F, and Class Φ_2, are widely adopted, which improve the systems' efficiency and reliability. However, the practical performance of conventional resonant inverters is limited to some extent by their load-sensitive characteristics. If the actual load changes, the output power will change and the system efficiency will inevitably decrease [5], [6]. Although feedback control represents a potential solution for different loads, it requires a complex design in practice. Therefore, the key issue for high-frequency resonant inverters is to maintain constant ac output and soft switching over a wide range of loads [7].

Generally, impedance compression and dynamic matching technology are typically used in the multi-MHz range to match the variable load impedance to the desired fixed load range. For better compression effect, the impedance network is designed specially to match the input and output impedance [8]. Although the inverters can operate effectively at the wide loads around the design point, the impedance networks consist of large passive components that are bulky and inefficient [9].

To solve the above challenges, the load-independent technology was proposed in [10] and [11], which is a time-domain method to optimize the circuit parameters. By setting soft switching and constant ac output requirements, the accurate numerical relationship between circuit parameters can be obtained. Compared with the traditional frequency-domain method presented in [12], the time-domain method is more accurate because the waveform equations for voltage and current are derived and the circuit parameters are solved numerically [13]. The theoretical design parameters are more accurate, which is beneficial to provide effective guidance for the actual design.

Since the load-independent technology was first proposed in the Class E resonant inverter in [10], the parameter optimization design method has been gradually applied in other high-frequency resonant inverter topologies [13], [14], [15], [16], [17], [18], [19]. The more flexible design approach and detailed operating characteristics analysis for load-independent Class E inverters are proposed in [13], which further extends the load-independent concept to Class E/F topologies. Likewise, the Class E inverter with the parallel resonant filter was optimally designed based on the load-independent technology in [14], [15], [16]. Furthermore, the inverse Class E inverter with constant ac voltage output and zero-current switching characteristics is introduced in [17]. Furthermore, the duality of Class E and inverse Class E topologies with load-independent characteristics were analyzed in [18], which further proposed the topology construction strategy of the Class E resonant inverter. To reduce the EMI for the finite input inductor of the Class E topology, the above load-independent design can be applied in the Class E/F resonant inverters [13], [19]. Moreover, the high-order resonant networks of Class E/F inverters can effectively reduce the

Received 21 October 2024; revised 7 December 2024; accepted 29 December 2024. Date of publication 6 January 2025; date of current version 26 February 2025. This work was supported in part by the National Natural Science Foundation of China under Grant 52377175 and in part by the Delta Power Electronics Science and Education Development Program of Delta Group under Grant DREK2023003. Recommended for publication by Associate Editor H. H.-C. Iu. *(Corresponding author: Yueshi Guan.)*

Yi Cheng, Yueshi Guan, Jiachao Zong, Yijie Wang, and Dianguo Xu are with the School of Electrical Engineering and Automation, Harbin Institute of Technology, Harbin 150001, China (e-mail: 23b906015@stu.hit.edu.cn; guanyueshi@hit.edu.cn; 23s106151@stu.hit.edu.cn; wangyijie@hit.edu.cn; xudiang@hit.edu.cn).

Tingting Yao is with the College of Computer and Control Engineering, Northeast Forestry University, Harbin 150040, China (e-mail: yaotingting@nefu.edu.cn).

Color versions of one or more figures in this article are available at https://doi.org/10.1109/TPEL.2025.3525665.

Digital Object Identifier 10.1109/TPEL.2025.3525665

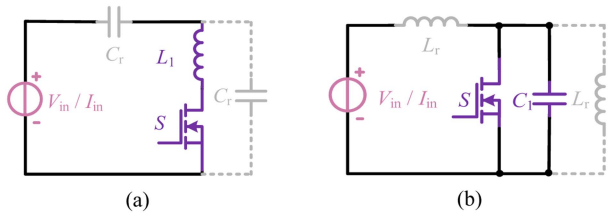

Fig. 1. (a) Class E^{-1} resonant unit. (b) Class E resonant unit.

voltage or current stress [20]. Therefore, the load-independent technology is widely applied in MHz wireless power transfer, which requires high power efficiencies and constant ac output in a wide load range [20], [21]. However, these traditional Class E/F inverters under load-independent design can only achieve constant ac current output [13], [19].

For high-frequency resonant converters, space plasma generation, etc., the constant ac voltage output characteristics are desirable. However, these Class EF resonant inverters under load-independent design only achieve constant ac current output. To expand the output characteristics, the common solution is adding the impedance networks in [15], which transfers constant ac current output to constant ac voltage output. To reduce the bulky passive components and voltage or current stress across the switch, the load-independent Class EF resonant topologies must be reconstructed for constant ac voltage output.

The contributions of this article are summarized as follows:

1) The load-independent topology construction method is extended from Class E topologies to Class EF topologies and a family of novel Class EF resonant topologies with constant ac voltage output are proposed.
2) The load-independent parameter design method is further optimized for different Class EF deign procedures. The operating characteristics and duality relationships of the proposed Class EF topologies are concluded.
3) The power output capability is further optimized. The designed prototype can achieve zero-voltage switching (ZVS) over a wide load range and higher peak power output capability.

This article is structured as follows: Section II summarizes the topology design principle and proposes a family of load-independent Class EF resonant inverters with constant ac voltage output. Section III introduces the common-ground Class EF resonant inverter as an example and provides a detailed time-domain analysis, load-independent design, power output capability, and loss analysis. Section IV presents the experimental results and comparisons of the proposed inverter. Finally, Section V concludes this article.

II. Topology Design Principle

As shown in Fig. 1, the Class E unit is divided into Class E^{-1} and Class E resonant units. To achieve soft switching, the resonant inductor L_1 is series with switch S for zero-current switching in the Class E^{-1} resonant unit. The capacitor C_r generally has two possible locations in the Class E^{-1} resonant unit, which resonates with inductor L_1. Likewise, the resonant capacitor C_1 is parallel with the switch S for ZVS in the Class E resonant unit. The inductor L_r generally also has two possible locations in the Class E resonant unit, which resonates with capacitor C_1. To reduce the voltage or current stress across the switch, the second-order resonant networks (L_2, C_2) are added to replace the resonant inductor L_r and capacitor C_r respectively, in traditional Class E^{-1} and Class E resonant units, which are defined as Class EF topologies.

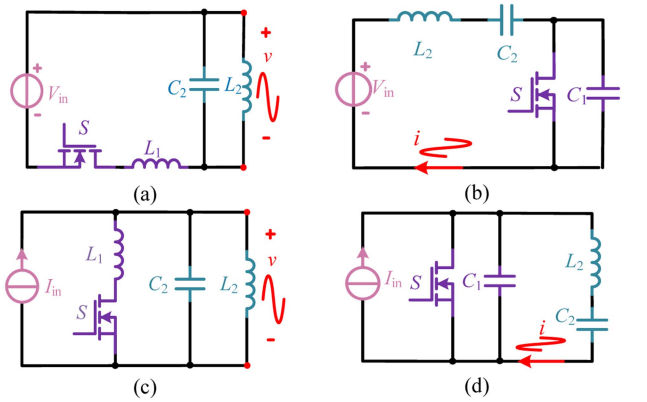

Fig. 2. (a) Class F/E unit series with second-order network. (b) Class E/F unit series with second-order network. (c) Class F/E unit parallel with second-order network. (d) Class E/F unit parallel with second-order network.

As shown in Fig. 2, the Class EF resonant units are constructed based on Class E resonant units and second-order resonant networks (L_2, C_2). To reduce the current stress across the switch, the inductor L_2 and capacitor C_2 are in parallel to construct a low-impedance loop for higher-order current harmonics in Class F/E resonant units. Likewise, to reduce the voltage stress across the switch, the inductor L_2 and capacitor C_2 are in series to construct a low-impedance loop for higher-order voltage harmonics in Class E/F resonant units. Generally, q_2 represents the frequency ratio of the second-order resonant network to switching frequency, that is,

$$q_2 = \frac{f_2}{f_S} = \frac{1}{\omega\sqrt{L_2C_2}} = \frac{1}{2\pi f_S\sqrt{L_2C_2}}. \tag{1}$$

Similar to the Class E unit, the Class EF resonant unit is divided into Class E/F and Class F/E resonant units according to soft switching characteristics. Obviously, zero-current switching can be achieved by the Class F/E resonant unit and ZVS can be achieved by the Class E/F resonant unit. Generally, q_1 represents the frequency ratio of the Class EF resonant unit to the switching frequency, that is,

$$q_1 = \begin{cases} \frac{1}{\omega\sqrt{L_2C_2}}\sqrt{\frac{L_1+L_2}{L_1}} = q_2\sqrt{\frac{L_1+L_2}{L_1}} \text{ (Class F/E)} \\ \frac{1}{\omega\sqrt{L_2C_2}}\sqrt{\frac{C_1+C_2}{C_1}} = q_2\sqrt{\frac{C_1+C_2}{C_1}} \text{ (Class E/F)} \end{cases}. \tag{2}$$

The ac voltage or current output can be obtained with high-load quality factor filters. Through the reasonable combination of Class EF resonant units and filter units, a family of Class EF resonant inverters with constant ac voltage output

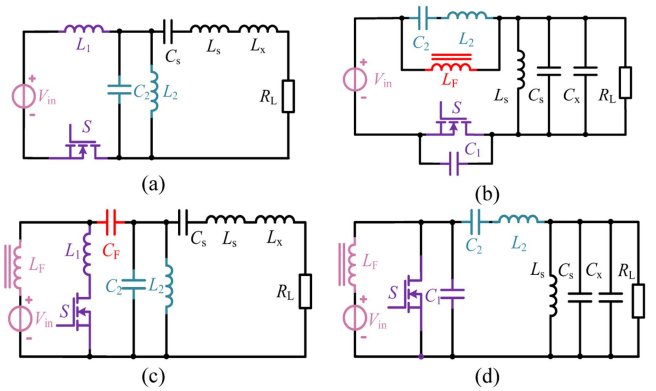

Fig. 3. (a) Floating-ground Class F/E inverter. (b) Floating-ground class E/F inverter. (c) Common-ground Class F/E inverter. (d) Common-ground Class E/F inverter.

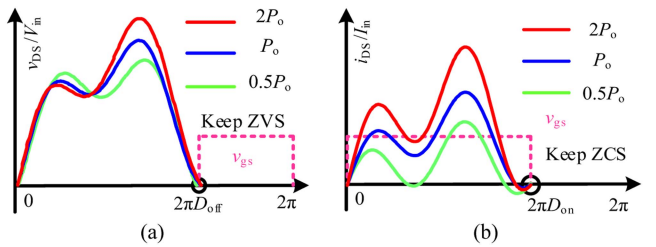

Fig. 4. Soft-switching waveforms of the Class EF inverters under load-independent design. (a) Zero-voltage switching. (b) Zero-current switching.

and load-independent characteristics can be obtained in Fig. 3. The extra choke inductor L_{F} and dc-blocking capacitor C_{F} are added, respectively, in Fig. 3(b) and (d) for volt–second and ampere–second balance. These Class EF resonant inverters are classified into floating-ground and common-ground types based on the configuration relationship between the switch and the load. Through comparing the time-domain theoretical waveform equations and operating characteristics, the Class F/E inverter in Fig. 3(a) is dual to the Class E/F inverter in Fig. 3(d). Likewise, the Class E/F inverter in Fig. 3(b) is dual to the Class F/E inverter in Fig. 3(c).

As shown in Fig. 4, these Class EF resonant inverters under load-independent design can achieve soft switching over a wide load range. For constant ac output and high efficiency, the circuit parameters must be optimized and the detailed design requirements are as follows.

a) *Low voltage or current stress across the switch:* The resonant frequency f_2 of the second-order resonant network (L_2, C_2) is typically one to two times the switching frequency f_{S}

$$q_2 = \frac{1}{\omega\sqrt{L_2 C_2}} = \frac{f_2}{f_{\mathrm{S}}} = 1 \sim 2. \tag{3}$$

b) *Zero current or voltage switching:* Soft switching should be achieved for high efficiency as shown in Fig. 4.

$$v_{\mathrm{S}}\left(2\pi D_{\mathrm{OFF}}\right) = 0 \mathrm{or} i_{\mathrm{S}}\left(2\pi D_{\mathrm{ON}}\right) = 0. \tag{4}$$

c) *Constant ac voltage output:* The ac output voltage V_{m} is unbiased with respect to the load R_{L}

$$\frac{\partial V_m}{\partial R_{\mathrm{L}}} = 0. \tag{5}$$

The time-domain theoretical waveform equation of voltage and current must be calculated. Based on the theoretical waveform equation, the soft switching requirement (b) can be simplified and the generic equations between input voltage, output voltage, and load R_{L} can be obtained as follows:

$$\Phi_q\left(D, q_2, q_1\right) V_{\mathrm{m}} = \Phi_\phi\left(D, q_2, q_1, \phi\right) V_{\mathrm{in}} R_{\mathrm{L}} \tag{6}$$

where ϕ is the phase difference between output voltage and drive signal, and the coefficient equations $\Phi_{\mathrm{q}}(D, q_2, q_1)$ and $\Phi_\phi(D, q_2, q_1, \phi)$ are too complex and omitted.

To achieve constant ac voltage output in requirement (c), the coefficients of (6) must be zero and the output ac voltage can be decoupled from the load R_{L}. Therefore, the frequency and phase conditions can be calculated as shown in (7). Finally, the simplified frequency condition and phase condition are shown in Table I.

$$\Phi_q\left(D, q_2, q_1\right) = \Phi_\phi\left(D, q_2, q_1, \phi\right) = 0. \tag{7}$$

Obviously, these load-independent topologies are dual. By exchanging the voltage terms with the current terms and exchanging the inductance terms with the capacitance terms, the time domain theoretical waveform equations of these load-independent Class EF resonant inverters can be derived easily. Therefore, the operating characteristics and load-independent parameter design can be derived by analogy according to the duality properties for simplicity.

Table I shows the operating characteristics of the proposed Class EF resonant inverters with constant ac voltage output under the load-independent design. The simplified expression of circuit gain is shown in (8), at the bottom of the next page. By exchanging ON-duty cycle D_{ON} with OFF-duty cycle D_{OFF}, these load-independent Class EF resonant inverters share common frequency conditions, circuit gain, and similar phase conditions. For the same operating and output characteristics, the load-independent Class F/E resonant inverters in Fig. 3(a) and (c) can share the same circuit design parameters. This design rule is also suitable for the load-independent Class E/F resonant inverters in Fig. 3(b) and (d).

Obviously, the Class E/F resonant inverters are competitive under high voltage output conditions for ZVS. On the contrary, the Class F/E resonant inverters are suitable for high current output conditions for zero-current switchings. Moreover, the parallel filter can improve the system efficiency and power density for less inductance. To simplify the drive circuit, the common-ground configuration is a common choice.

TABLE I
OPERATING CHARACTERISTICS OF THE PROPOSED LOAD-INDEPENDENT CLASS E/F RESONANT INVERTERS

Topology	Fig. 3(a)	Fig. 3(b)	Fig. 3(c)	Fig. 3(d)
Resonant unit	Class F/E	Class E/F	Class F/E	Class E/F
Output filter unit	Series filter	Parallel filter	Series filter	Parallel filter
Duty cycle D	On-duty cycle D_{on}	Off-duty cycle D_{off}	On-duty cycle D_{on}	Off-duty cycle D_{off}
Soft switching	Zero current switching	Zero voltage switching	Zero current switching	Zero voltage switching
Output characteristics	Constant ac voltage output			
Frequency condition	$\frac{1}{q_2\tan[\pi(D-1)q_2]}-\frac{1}{q_1\tan(\pi Dq_1)}=\frac{q_1^2-q_2^2}{\pi Dq_1^2q_2^2}$ ($D=D_{off}$ for Class E/F, $D=D_{on}$ for Class F/E)			
Phase condition	$\phi=\pi\left(\frac{1}{2}-D_{on}\right)$	$\phi=\pi\left(\frac{3}{2}-D_{off}\right)$	$\phi=\pi\left(\frac{3}{2}-D_{on}\right)$	$\phi=\pi\left(\frac{1}{2}-D_{off}\right)$
Operating characteristics	$G_v=\frac{V_m}{V_{in}}=\Phi_{Gain}(D_{on},q_1,q_2)$	$G_i=\frac{I_m}{I_{in}}=\Phi_{Gain}(D_{off},q_1,q_2)$	$G_v=\frac{V_m}{V_{in}}=\Phi_{Gain}(D_{on},q_1,q_2)$	$G_i=\frac{I_m}{I_{in}}=\Phi_{Gain}(D_{off},q_1,q_2)$
	Maximum output power capability $C_p=0.1083$ (duty cycle D =0.596, the second-order resonant frequency q_2 = 1.07 and load factor p = 8.56)			

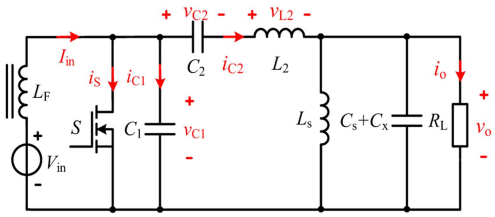

Fig. 5. Topology of the load-independent common-ground Class E/F resonant inverter with constant ac voltage output.

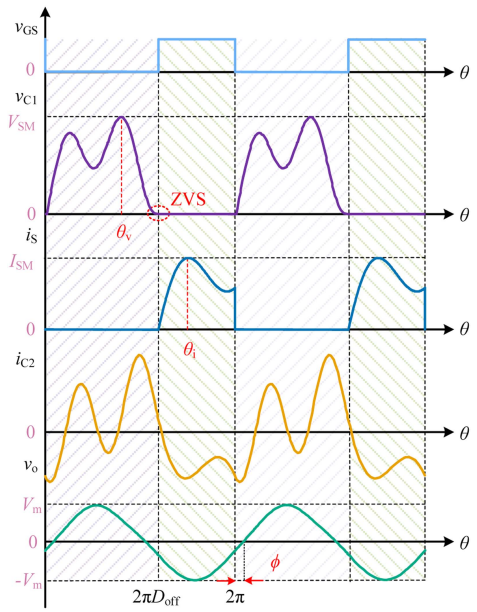

Fig. 6. Main voltage and current waveforms when load-independent common-ground Class E/F inverter achieves maximum output power capability.

III. LOAD-INDEPENDENT ANALYSIS AND DESIGN OF THE PROPOSED INVERTER

A. Circuit Analysis

The common-ground Class E/F resonant inverter is taken as an example to validate the load-independent theory. Fig. 5 shows the topology of the common-ground Class E/F resonant inverter consisting of the input voltage source V_{in}, the input choke inductor L_F, the switch S, the second-order resonant network (L_2, C_2), the resonant capacitor C_1, the parallel output filter (C_s, C_x, L_s), and the load resistance R_L. The special case when the load-independent common-ground Class E/F resonant inverter achieves maximum output power capability is shown in Fig. 6, where D_{OFF} is the OFF-duty cycle of the switching device and $\theta=\omega t=2\pi f_S t$ is the angular shift.

To simplify the time-domain analysis, the assumptions are made as follows.

$$\Phi_{Gain}(D,q_1,q_2)=\frac{8q_2(q_1^2-q_2^2)\left(q_1\cos(\pi Dq_1)\sin(\pi(D-1)q_2)-q_2\sin(\pi Dq_1)\cos(\pi(D-1)q_2)\right)}{\pi q_1(q_1^2-1)(q_2^2-1)\left((q_1+q_2)^2\cos(2\pi(D(q_1-q_2)+q_2))-(q_1-q_2)^2(\cos(2\pi(D(q_1+q_2)-q_2)))-4q_1q_2\right)}$$
$$(\sin(\pi Dq_1)\left((q_2-1)(q_1^2+q_2)\sin(\pi((D-1)q_2+D))+(q_2+1)(q_1^2-q_2)\sin(\pi(D(1-q_2)+D))\right)$$
$$-2q_1(q_2^2-1)\sin(\pi D)\cos(\pi Dq_1)\sin(\pi(D-1)q_2)) \quad (8)$$

1) The quality factor of the parallel output filter is high enough to form a sinusoidal output current and voltage

$$v_{\rm o}=V_{\rm m}\sin(\theta+\phi)=I_{\rm m}R_{\rm L}\sin(2\pi f_{\rm S}t+\phi) \quad (9)$$

where $I_{\rm m}$ and $V_{\rm m}$ are the output ac current and voltage amplitude and $f_{\rm S}$ is the switching frequency.
2) The switch device is ideal, whose ON-resistance is zero and OFF-resistance is infinite. The parasitic capacitor is absorbed by the resonant capacitor C_1.
3) All the passive components are ideal and lossless, whose parasitic parameters are neglected.

OFF state [$0 \le \theta < 2\pi D_{OFF}$]: At time 0, the switch S has turned OFF. Obviously, the current across the switch $i_{\rm S}$ is zero and the voltage across the switch is equal to the resonant capacitor voltage v_{C1}. The voltage stress across the switch is reduced significantly by the second-order resonant network (L_2, C_2), which is low impedance for the second-order harmonics voltage. During this mode, the voltage across the switch reaches the peak value $V_{\rm SM}$ when the angular shift $\theta=\theta_{\rm v}$.

ON state [$2\pi D_{OFF} \le \theta < 2\pi$]: Once the driving signal arrives at $2\pi D_{\rm OFF}$, the switch S turns ON with zero voltage. During this mode, the voltage across the switch is zero and the current through the switch reaches the peak value $I_{\rm SM}$ when the angular shift $\theta=\theta_{\rm i}$. During this mode, the second-order network resonates with the parallel output filter unit.

In the OFF state, the circuit resonates in series. From Kirchhoff's voltage and current laws, the following relationships can be obtained:

$$\begin{cases} I_{\rm in}=i_{\rm C1}(\theta)+i_{\rm C2}(\theta) \\ v_{\rm C1}(\theta)=v_{\rm C2}(\theta)+v_{\rm L2}(\theta)+V_{\rm m}\sin(\theta+\phi) \end{cases}. \quad (10)$$

Rearranging (10), the second-order differential equation for the current through the resonant capacitor C_2 can be derived as

$$\omega^2 C_1 L_2\frac{{\rm d}^2 i_{\rm C2}(\theta)}{{\rm d}\theta^2}+\frac{C_1+C_2}{C_2}i_{\rm C2}(\theta) = I_{\rm in}-\omega C_1 V_m\cos(\theta+\phi). \quad (11)$$

The general solution and particular solution can be calculated based on (11). The expression for the current through capacitor C_2 during the OFF state can be obtained as follows:

$$i_{\rm C2}(\theta)=A_1\sin q_1\theta+A_2\cos q_1\theta+\frac{1}{1-q_1^2}\frac{V_{\rm m}}{\omega L_2}\cos(\theta+\phi)+\frac{q_1^2-q_2^2}{q_1^2}I_{\rm in} \quad (12)$$

where the coefficients A_1 and A_2 are determined by the initial operating conditions.

According to the operating characteristics of the capacitor, the expression for the voltage across the switch S can be calculated as follows:

$$v_{\rm C1}(\theta)=\frac{1}{\omega C_1}\int_0^\theta[I_{\rm in}-i_{\rm C2}(\theta)]{\rm d}\theta+v_{\rm C1}(0) =\frac{(q_1^2-q_2^2)\omega L_2}{q_1}\left\{A_1(\cos q_1\theta-1)-A_2\sin q_1\theta+\frac{q_2^2 I_{\rm in}}{q_1}\theta -\frac{q_1}{1-q_1^2}\frac{V_{\rm m}}{\omega L_2}[\sin(\theta+\phi)-\sin\phi]\right\}+v_{\rm C1}(0). \quad (13)$$

From Kirchhoff's current law, the following relationships can be obtained in the ON state:

$$\begin{cases} v_{\rm C1}(\theta)=0 \\ v_{\rm L2}+v_{\rm C2}+V_{\rm m}\sin(\theta+\phi)=0 \end{cases}. \quad (14)$$

Rearranging (14), the second-order differential equation for the voltage across the resonant capacitor C_2 can be obtained as follows:

$$\omega^2 L_2 C_2\frac{{\rm d}^2 v_{\rm C2}(\theta)}{{\rm d}\theta^2}+v_{\rm C2}(\theta)+V_{\rm m}\sin(\theta+\phi)=0. \quad (15)$$

Likewise, the expression for the voltage across the capacitor C_2 during the ON state can be calculated as follows:

$$v_{\rm C2}(\theta)=B_1\sin q_2\theta+B_2\cos q_2\theta+\frac{q_2^2}{1-q_2^2}V_{\rm m}\sin(\theta+\phi) \quad (16)$$

where the coefficients B_1 and B_2 are determined by the initial operating conditions.

From (1) and (2), the relationship between the capacitors C_1 and C_2 is determined by the resonant frequency q_1 and q_2 as follows:

$$\frac{C_1}{C_2}=\frac{q_2^2}{q_1^2-q_2^2}. \quad (17)$$

According to the operating characteristics of the capacitor, the expression for the current through the resonant capacitor C_2 during the ON state can be obtained as follows:

$$i_{\rm C2}(\theta)=\omega C_2\frac{{\rm d}v_{\rm C2}(\theta)}{{\rm d}\theta} =\frac{1}{q_2^2\omega L_2}\left[B_1 q_2\cos q_2\theta-B_2 q_2\sin q_2\theta+\frac{q_2^2}{1-q_2^2}V_{\rm m}\cos(\theta+\phi)\right]. \quad (18)$$

From Kirchhoff's voltage law, the expression for the current through the switch S can be obtained as follows:

$$i_{\rm S}(\theta)=I_{\rm in}-i_{\rm C2}(\theta). \quad (19)$$

In all, the theoretical voltage and current expressions of the switch and resonant elements in one cycle are summarized as follows:

$$i_{\rm S}(\theta)= \begin{cases} 0 & [0\le\theta<2\pi D_{\rm OFF}] \\ I_{\rm in}-\frac{1}{q_2^2\omega L_2}\left[\frac{q_2^2}{1-q_2^2}V_{\rm m}\cos(\theta+\phi)\right. & \\ \left.+B_1 q_2\cos q_2\theta-B_2 q_2\sin q_2\theta\right] & [2\pi D_{\rm OFF}\le\theta<2\pi] \end{cases} \quad (20)$$

$$v_{\rm C1}(\theta)=$$

$$\begin{cases} \frac{\left(q_1^2-q_2^2\right)\omega L_2}{q_1}\left\{A_1\left(\cos q_1\theta-1\right)-A_2\sin q_1\theta \right. \\ \left. +\frac{q_2^2 I_{\text{in}}}{q_1}\theta-\frac{q_1}{1-q_1^2}\frac{V_{\text{m}}}{\omega L_2}\left[\sin\left(\theta+\phi\right)-\sin\phi\right]\right\} & [0\le\theta<2\pi D_{\text{OFF}}] \\ 0 & [2\pi D_{\text{OFF}}\le\theta<2\pi] \end{cases} \tag{21}$$

$$v_{\text{C2}}(\theta)=$$

$$\begin{cases} \frac{q_2^2\omega L_2}{q_1}\left\{\frac{\left(q_1^2-q_2^2\right)I_{\text{in}}}{q_1}\theta+A_1\left(1-\cos q_1\theta\right) \right. \\ \left. +A_2\sin q_1\theta+\frac{q_1}{1-q_1^2}\frac{V_{\text{m}}}{\omega L_2}\left[\sin\left(\theta+\phi\right)-\sin\phi\right]\right\} \\ \qquad\qquad [0\le\theta<2\pi D_{\text{OFF}}] \\ B_1\sin q_2\theta+B_2\cos q_2\theta+\frac{q_2^2}{1-q_2^2}V_{\text{m}}\sin\left(\theta+\phi\right) \\ \qquad\qquad [2\pi D_{\text{OFF}}\le\theta<2\pi] \end{cases} \tag{22}$$

$$i_{\text{C2}}(\theta)=$$

$$\begin{cases} A_1\sin q_1\theta+A_2\cos q_1\theta+\frac{q_1^2-q_2^2}{q_1^2}I_{\text{in}} & [0\le\theta<2\pi D_{\text{OFF}}] \\ +\frac{1}{1-q_1^2}\frac{V_{\text{m}}}{\omega L_2}\cos\left(\theta+\phi\right) & \\ \frac{1}{q_2^2\omega L_2}\left[\frac{q_2^2}{1-q_2^2}V_{\text{m}}\cos\left(\theta+\phi\right)\right. & [2\pi D_{\text{OFF}}\le\theta<2\pi] \\ \left.+B_1 q_2\cos q_2\theta-B_2 q_2\sin q_2\theta\right] & \end{cases} . \tag{23}$$

The coefficients A_1, A_2, B_1, and B_2 can be calculated by solving the boundary continuity equations at the turn ON and turn OFF switching instants. The boundary conditions can be obtained because the voltage across the capacitor v_{C2} and the current through the capacitor i_{C2} are continuous.

$$\begin{cases} v_{\text{C2}}(0)=v_{\text{C2}}(2\pi) \\ v_{\text{C2}}\left(2\pi D_{\text{OFF}}^{-}\right)=v_{\text{C2}}\left(2\pi D_{\text{OFF}}^{+}\right) \\ i_{\text{C2}}(0)=i_{\text{C2}}(2\pi) \\ i_{\text{C2}}\left(2\pi D_{\text{OFF}}^{-}\right)=i_{\text{C2}}\left(2\pi D_{\text{OFF}}^{+}\right) \end{cases} . \tag{24}$$

B. Parameter Design for Load-Independent Operation

To achieve the load-independent characteristics, soft switching condition (b) must be satisfied regardless of load variation. Substituting (21) into (4), the relationship between the output voltage V_{m} and load resistance R_{L} can be obtained as follows:

$$\Phi_q\left(D_{\text{OFF}},q_2,q_1\right)V_{\text{m}}=\Phi_\phi\left(D_{\text{OFF}},q_2,q_1,\phi\right)V_{\text{in}}R_{\text{L}} \tag{25}$$

Furthermore, the frequency condition (26) and phase condition (27) for the load-independent characteristic can be obtained as follows:

$$\frac{1}{q_2\tan[\pi(D_{\text{OFF}}-1)q_2]}-\frac{1}{q_1\tan(\pi D_{\text{OFF}}q_1)}=\frac{q_1^2-q_2^2}{\pi D_{\text{OFF}}q_1^2q_2^2} \tag{26}$$

$$\phi=\pi\left(\frac{1}{2}-D_{\text{OFF}}\right). \tag{27}$$

The frequency condition (26) is a multiparameter nonlinear equation, which is a common characteristic for all the load-independent Class EF resonant inverters.

Substituting the frequency and phase conditions into the calculated theoretical expressions, the relationship between the circuit parameters can be derived. The current of the resonant capacitor C_2 is subjected to the Fourier analysis, and the fundamental frequency component of the current through the parallel output filter can be expressed as follows:

$$\begin{aligned} i_{\text{C2}}(\theta)&=i_{\text{o}}(\theta)+i_{\text{Cx}}(\theta) \\ &=I_{\text{m}}\sin(\theta+\phi)+\omega C_{\text{x}}V_{\text{m}}\cos(\theta+\phi) \\ &=I_{\text{m}}\sin(\theta+\phi)+I_{\text{Cx}}\cos(\theta+\phi) \end{aligned} \tag{28}$$

where I_{Cx} is the amplitude of the current through capacitor I_{Cx}.

Based on (28), the current through the load resistance and the residual impedance in the parallel output filter unit can be calculated as follows:

$$I_{\text{m}}=\frac{1}{\pi}\int_0^{2\pi}i_{\text{C2}}\left(\theta\right)\sin(\theta+\phi)\text{d}\theta \tag{29}$$

$$I_{\text{Cx}}=\omega C_{\text{x}}V_{\text{m}}=\frac{1}{\pi}\int_0^{2\pi}i_{\text{C2}}\left(\theta\right)\cos(\theta+\phi)\text{d}\theta. \tag{30}$$

By simplifying (29), the voltage gain G_{v} and the current gain G_{i} of the load-independent common-ground Class E/F resonant inverter can be calculated as follows:

$$G_{\text{i}}=\frac{I_{\text{m}}}{I_{\text{in}}}=\frac{2V_{\text{in}}}{V_{\text{m}}}=\frac{2}{G_{\text{v}}}=\Phi_{\text{Gain}}\left(D_{\text{OFF}},q_1,q_2\right). \tag{31}$$

Likewise, the relationship between resonant inductor L_2 and residual capacitor C_{x} can be derived by simplifying (30) as follows:

$$\omega^2L_2C_{\text{x}}=\Phi_{\text{Cx}}\left(D_{\text{OFF}},q_1,q_2\right) \tag{32}$$

where $\Phi_{\text{Cx}}(D_{\text{OFF}}, q_1, q_2)$ is emitted for extremely complex functions determined by resonant parameters.

Based on the above analysis, the circuit parameter relationship of the proposed common-ground Class E/F resonant inverter is determined. Once the OFF-duty cycle D_{OFF} and the resonant frequency ratio q_2 are determined, only a set of unique solutions exist for the resonant frequency ratio q_1, the phase difference ϕ, and the current gain G_{i}. Furthermore, the residual capacitor C_{x} and filter inductor L_{s} in the parallel output filter unit can be fixed according to the designed load quality Q. Fig. 7 shows the solutions for the design parameters with different OFF-duty cycle D_{OFF} and resonant frequency ratio q_2 for the load-independent common-ground Class E/F resonant inverter, which is also suitable for other dual Class EF topologies. Therefore, the general value range of the resonant frequency ratio q_1 is 2∼3 and the current gain G_{i} is 1∼2, respectively.

C. Power Output Capability Analysis

To scale the load variation with respect to the resonance parameters, the parameter load factor p is introduced, which is defined as follows:

$$p=\frac{1}{\omega L_2}\frac{V_{\text{m}}}{I_{\text{in}}}=\frac{R_{\text{L}}}{\omega L_2}\frac{I_{\text{m}}}{I_{\text{in}}}. \tag{33}$$

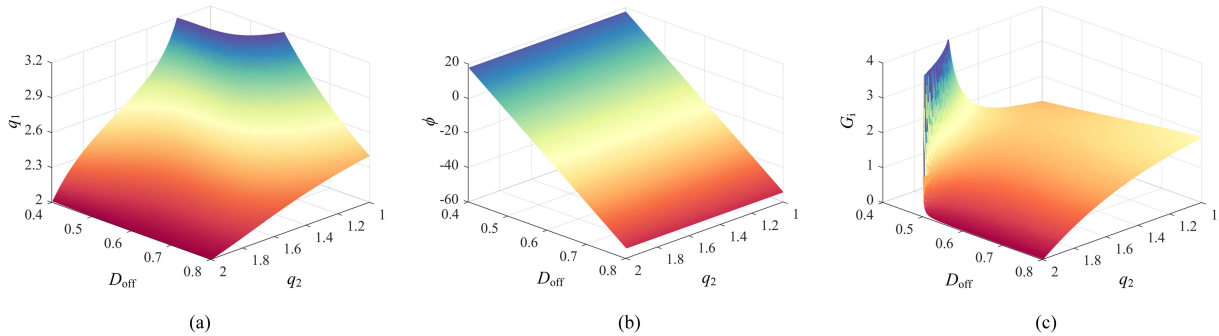

Fig. 7. Design parameters for the load-independent common-ground Class E/F inverter with the different OFF-duty cycle D_{OFF} and the second-order resonant frequency ratio q_2. (a) Resonant frequency ratio q_1. (b) Phase difference ϕ. (c) Current gain G_i.

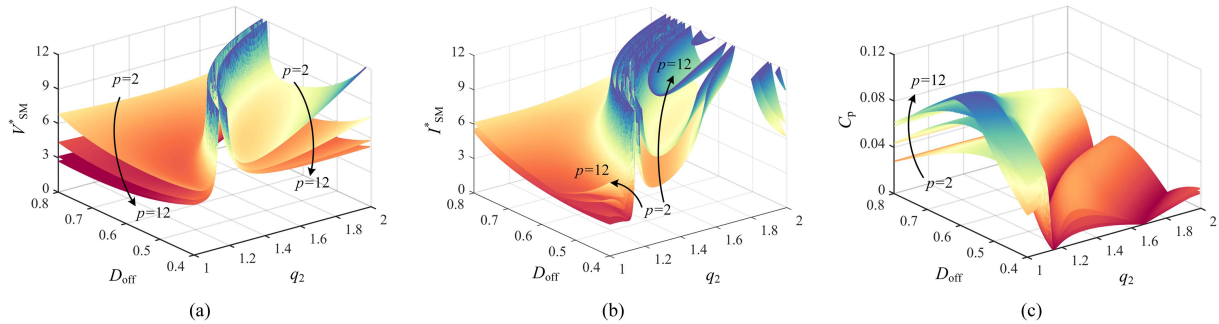

Fig. 8. Operating characteristics for the load-independent common-ground Class E/F resonant inverter with the different OFF-duty cycle D_{OFF} and the second-order resonant frequency ratio q_2 under the different load factor p from 2 to 12. (a) Voltage stress across the switch. (b) Current stress through the switch. (c) Power output capability.

According to the detailed theoretical expressions for the switch voltage and current stress, the peak voltage stress value and current stress value of the switch can be calculated at θ_v and θ_i, respectively, as follows:

$$\begin{cases} \left.\frac{\mathrm{d}v_S(\theta_v)}{\mathrm{d}\theta}\right|_{\theta=\theta_v} = 0 \\ 0 < \theta_v \le 2\pi D_{OFF} \end{cases} \text{and} \begin{cases} \left.\frac{\mathrm{d}i_S(\theta_i)}{\mathrm{d}\theta}\right|_{\theta=\theta_i} = 0 \\ 2\pi D_{OFF} < \theta_i \le 2\pi \end{cases}. \quad (34)$$

Based on (21) and (34), the angular displacement θ_v for the maximum voltage stress can be calculated as follows:

$$\frac{A_1}{I_m}\sin q_1\theta_v + \frac{A_2}{I_m}\cos q_1\theta_v + \frac{1}{1-q_1^2}\frac{p}{G_i}\cos(\theta_v+\phi) = \frac{q_2^2}{q_1^2}\frac{1}{G_i}. \quad (35)$$

Based on (20) and (35), the angular displacement θ_i for the maximum current stress can be calculated as follows:

$$\frac{B_1}{V_m}\sin q_2\theta_i + \frac{B_2}{V_m}\cos q_2\theta_i + \frac{1}{1-q_2^2}\sin(\theta_i+\phi) = 0. \quad (36)$$

Therefore, the power output capability C_p of the proposed load-independent common-ground Class E/F inverter can be obtained as follows:

$$C_p = \frac{P_{in}}{V_{SM}I_{SM}} = \frac{V_{in}I_{in}}{V_{SM}I_{SM}} = \frac{1}{\frac{V_{SM}}{V_{in}}\frac{I_{SM}}{I_{in}}} = \frac{1}{V^*_{SM}I^*_{SM}}. \quad (37)$$

Based on mathematical computing software, high-order nonlinear equations can be programmed and solved with iterative and gradient descent algorithms. Furthermore, the voltage stress and current stress across the switch at different OFF-duty cycles D_{OFF}, resonant frequency q_2, and load factor p can be obtained as shown in Fig. 8(a) and (b). Furthermore, Fig. 8(c) shows the power output capability of the proposed load-independent common-ground Class E/F resonant inverter. To reduce the switch voltage stress and improve power output capability, the reasonable design range for the second-order resonant frequency q_2 is around 1.1. In this case, the voltage stress decreases and the current stress increases with the load factor p increasing. Moreover, the power output capability reaches the peak value $C_p = 0.1083$ when the OFF-duty cycle $D_{OFF} = 0.596$, the second-order resonant frequency $q_2 = 1.07$, and the load factor $p = 8.56$. Therefore, the reasonable value range of the resonant frequency ratio q_2 is $1 \sim 1.2$ and the OFF-duty cycle D_{OFF} is $0.5 \sim 0.7$, respectively. For the initial purpose of reducing current stress, the proposed load-independent common-ground Class E/F inverter is suitable for step-up and high-input voltage situations.

IV. Experiments and Comparison

A. Experimental Verification

Based on the above load-independent analysis and design, the step-by-step inverter parameter design procedure is presented and the detailed designed specifications are as follows:

1) the switching frequency $f_S = 1$ MHz;
2) the dc voltage power supply $V_{in} = 25$ V;

3) the rated load resistance $R_{\rm L} = 25\,\Omega$;
4) the rated output voltage $V_{\rm m} = 35\,{\rm V}$;
5) the load quality factor $Q = 5.5$.

To achieve the highest power output capability, the OFF-duty cycle is $D_{\rm OFF} = 0.596$, the resonant frequency ratio of the second-order networks is $q_2 = 1.070$, and the load factor is $p = 8.560$ according to the operating characteristics analysis in Section III. Furthermore, the resonant frequency is $q_1 = 3.097$ and the phase difference is $\phi = $ -17.280 deg based on the frequency and phase condition. Finally, the voltage gain is $G_{\rm i} = 1.563$ based on (8).

According to design specifications and (33), the value of the resonant inductor L_2 can be calculated as follows:

$$L_2 = \frac{1}{\omega p}\frac{V_{\rm m}}{I_{\rm in}} = \frac{G_{\rm i}R_{\rm L}}{\omega p} = \frac{1.563 \times 25}{2 \times \pi \times 10^6 \times 8.56} = 0.727\mu{\rm H}. \tag{38}$$

According to (1), the value of the resonant capacitor C_2 can be obtained as follows:

$$C_2 = \frac{1}{q_2^2\omega^2 L_2} = \frac{1}{(1.07 \times 2 \times \pi \times 10^6)^2 \times 0.727 \times 10^{-6}} = 30.433{\rm nF}. \tag{39}$$

Moreover, the value of the resonant capacitor C_1 can be calculated based on (17) as follows:

$$C_1 = \frac{q_2^2 C_2}{q_1^2 - q_2^2} = \frac{(1.07)^2 \times 30.433 \times 10^{-9}}{(3.097)^2 - (1.07)^2} = 4.125{\rm nF}. \tag{40}$$

According to the definition of the load quality, the value of the filter capacitor in total can be obtained as follows:

$$C_{\rm total} = C_{\rm s}{+}C_{\rm x} = \frac{Q}{\omega R_{\rm L}} = \frac{5.5}{2 \times \pi \times 10^6 \times 25} = 35.014{\rm nF}. \tag{41}$$

To achieve constant ac voltage output, the value of the residual capacitor $C_{\rm x}$ can be obtained based on (32) as follows:

$$C_{\rm x} = \frac{\Phi_{\rm Cx}(D_{\rm OFF}, q_1, q_2)}{\omega^2 L_2} = \frac{-0.1391}{(2 \times \pi \times 10^6)^2 \times 0.727 \times 10^{-6}} = -4.847{\rm nF}. \tag{42}$$

Furthermore, the value of the parallel resonant capacitor $C_{\rm s}$ can be obtained as follows:

$$C_{\rm s} = C_{\rm total} - C_{\rm x} = 35.014 \times 10^{-9} - \left(-4.847 \times 10^{-9}\right) = 39.861{\rm nF}. \tag{43}$$

Finally, the value of the parallel resonant inductor $L_{\rm s}$ can be calculated as follows:

$$L_{\rm s} = \frac{1}{\omega^2 C_{\rm s}} = \frac{1}{(2 \times \pi \times 10^6)^2 \times 39.861 \times 10^{-9}} = 0.635\mu{\rm H}. \tag{44}$$

As shown in Fig. 9(a), the prototype of the load-independent common-ground Class E/F resonant inverter is implemented based on the above-designed component values. According to the duality of these topologies, the common-ground Class E/F resonant inverter and floating-ground Class E/F resonant inverter share the same circuit parameters and operating characteristics.

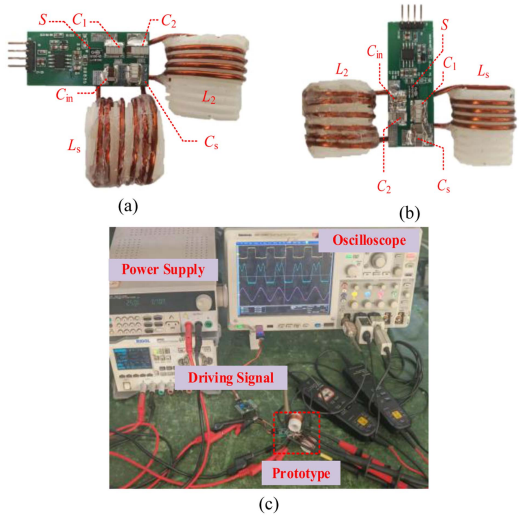

Fig. 9. (a) Picture of the common-ground Class E/F resonant inverter prototype. (b) Picture of the floating-ground Class E/F resonant inverter prototype. (c) Experimental measurement platform.

TABLE II
PARAMETERS OF MAIN COMPONENTS

Component	Value/Parameter
$L_{\rm F}$	Coilcraft, 150 μH
C_1	Murata 4.02 nF
C_2	Murata 30.45 nF
$C_{\rm total}$ ($C_{\rm s}$+$C_{\rm x}$)	Murata 35.00 nF
L_2	AWG 14, 0.73 μH, Q = 112 @ 1 MHz
$L_{\rm s}$	AWG 14, 0.63 μH, Q = 120 @ 1 MHz
Driver	Si8271
Switch S	GS61004B

The prototype of the floating-ground Class E/F resonant inverter and the experimental platform are, respectively, implemented as shown in Fig. 9(b) and (c). Table II shows the detailed component values and parameters. To improve system efficiency, all the resonant inductors are air-cored and hand-wound with 14 AWG wires. Additionally, resonant capacitors made of low-loss C0G ceramic capacitors from Murata are selected. Considering the switch parasitic capacitance $C_{\rm ds} = 100$ pF, the actual resonant capacitor C_1 is 4.02 nF. The input choke inductor under the PCB is selected from Coilcraft for low dc resistance.

Fig. 10 shows the experimental waveforms of the load-independent common-ground Class E/F resonant inverter with load resistances of 25, 50, 100, and 500 Ω. There is some distortion in ac output voltage for the low load quality Q. Obviously, the amplitude of output ac voltage remains constant at approximately 35 V when the load resistance changes from 25 to 500 Ω. Additionally, the voltage across the switch becomes zero when the switch turns ON, which improves the system's overall efficiency. These experimental results confirm the load-independent characteristics of the designed common-ground Class E/F resonant inverter.

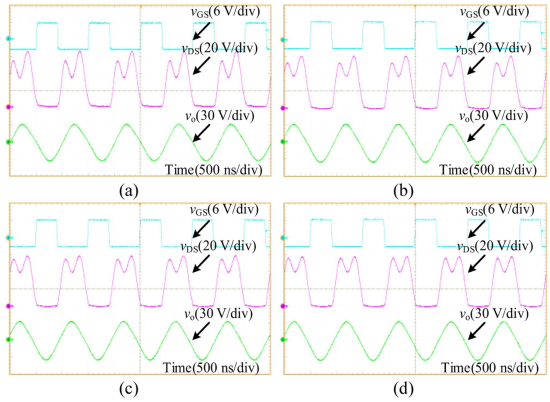

Fig. 10. Experimental waveforms of common-ground Class E/F inverter under different load resistances. (a) Load resistance $R_{\rm L} = 25\,\Omega$. (b) Load resistance $R_{\rm L} = 50\,\Omega$. (c) Load resistance $R_{\rm L} = 100\,\Omega$. (d) Load resistance $R_{\rm L} = 500\,\Omega$.

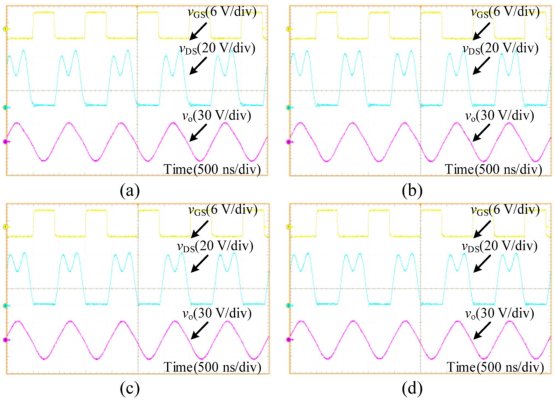

Fig. 11. Experimental waveforms of floating-ground Class E/F inverter under different load resistances. (a) Load resistance $R_L = 25\,\Omega$. (b) Load resistance $R_L = 50\,\Omega$. (c) Load resistance $R_L = 100\,\Omega$. (d) Load resistance $R_L = 500\,\Omega$.

Fig. 11 shows the experimental waveforms of the load-independent floating-ground Class E/F resonant inverter with load resistances of 25, 50, 100, and 500 Ω. Obviously, the amplitude of output ac voltage remains constant at approximately 35 V when the load resistance changes from 25 to 500 Ω. Moreover, the designed floating-ground Class E/F resonant inverter can achieve soft switching and constant ac voltage output in a wide load range. The experimental results confirm that the common-ground Class E/F inverter and floating-ground Class E/F inverter can achieve the same operating characteristics under the same design parameters. There are differences in switch voltage waveforms for parasitic parameters and the nonlinearity of switch and passive components.

Fig. 12 shows the experimental waveforms when the load resistances change from 25 to 500 Ω and from 50 to 25 Ω. Obviously, the voltage stress across the switch reduces with the output power decreasing. When the load changes from 25 to 500 Ω, the amplitude of output ac current changes from 1.4 to 0.07 A, which is almost close to zero due to the large scale. When the load changes from 50 to 25 Ω, the amplitude of output ac current changes from 0.7 to 1.4 A. Although little

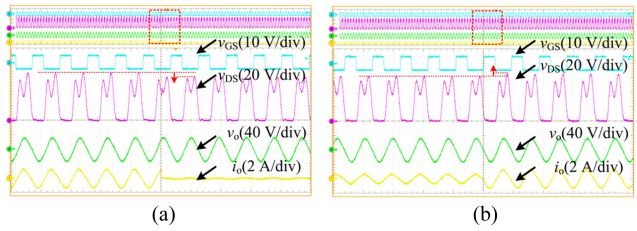

Fig. 12. Experimental waveforms of common-ground Class E/F inverter under load resistance change. (a) Load resistance changes from 25 to 500 Ω. (b) Load resistance changes from 50 to 25 Ω.

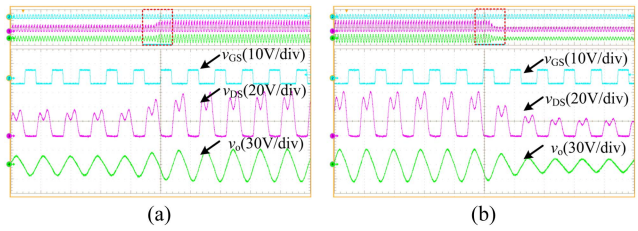

Fig. 13. Experimental waveforms of floating-ground Class E/F inverter under input voltage change. (a) Input voltage changes from 15 to 25 V. (b) Input voltage changes from 25 to 10 V.

change in voltage stress across the switch, ZVS and constant ac output voltage still remain. Obviously, the response speed is fast without close-loop control when the load resistance is switched.

Fig. 13 shows the experimental waveforms when the input voltage changes from 15 to 25 V and from 25 to 10 V. The output voltage amplitude changes from approximately 21 to 35 V and from 35 to 14 V, verifying that the voltage gain remains constant. Additionally, good soft-switching performance confirmed that ZVS can be maintained under different input voltages.

B. Comparison

The comparison of the load-independent topologies with constant ac output characteristics is shown in Table III. Although the Class Φ_2 resonant inverter in [9] can achieve the lowest voltage stress, the constant ac output characteristics are lost and the impedance network reduces the system efficiency. Compared with traditional load-independent Class E topologies in [14] and [15], the voltage stress can be significantly reduced for the second-order resonant networks of the Class E/F topologies despite the addition of passive components. The low voltage stress across the switch can improve the system efficiency and power output capability. Different from constant ac current output in [13], [14], [15], [16], [17], [18], and [19], the proposed load-independent Class E/F resonant inverter can achieve constant ac voltage output in a wide load range. The different output characteristic of the proposed load-independent Class E/F topology expands the application scenarios. For the inverters with zero-current switching characteristics in [18] and [19], the system efficiency slightly decreases for the current oscillation originating from the parasitic capacitance of the switch. However, ZVS and high efficiency can be achieved in

TABLE III
COMPARISON OF THE LOAD-INDEPENDENT HIGH-FREQUENCY RESONANT INVERTERS

Topology	Output Filter	Soft Switching	Constant Output	Component	V_{SMAX}/V_{in}	I_{SMAX}/I_{in}	Power Output Capability	Power (W)	Efficiency (%)	Operating Range (Ω)
Class Φ_2 [9]	Impedance Network	ZVS	-	4L+4C	2.17	4.90	0.094	22.5	90.0	25-250
Class E/F [13]	Series	ZVS	CC	3L+3C	2.25	5.05	0.088	150.0	90.0	0.56-6
Floating-ground Class E [14]	Parallel	ZVS	CC	2L+2C	3.48	3.16	0.091	10.0	89.3	1-40
Class E [15]	Impedance Network	ZVS	CC	3L+3C	3.78	2.59	0.102	10.4	88	1-8.6
Inverse Class E [18]	Series	ZCS	CC	3L+2C	2.61	3.74	0.102	19.5	93.8	0.25-5
Floating-ground Class F/E [19]	Parallel	ZCS	CC	3L+2C	4.12	4.05	0.061	25.0	94.2	5-50
This paper	Parallel	ZVS	CV	3L+3C	2.78	3.42	0.105	21.8	93.4	25-500

TABLE IV
COMPARISON OF THE PROPOSED LOAD-INDEPENDENT CLASS EF TOPOLOGIES WITH CONSTANT AC OUTPUT CHARACTERISTICS

Topology	Input current ripple	EMI	Passive component	Power density	Output configuration	Output filter	Soft switching	Application scenario
Fig. 3 (a)	Large	High	3L+2C	Middle	Floating-ground	Series filter	Zero-current turn-off	1. High input current 2. Wireless power transfer
Fig. 3 (b)	Large	High	3L+3C	Low	Floating-ground	Parallel filter	Zero-voltage turn-on	1. High frequency 2. High input voltage
Fig. 3 (c)	Small	Low	3L+3C	Low	Common-ground	Series filter	Zero-current turn-off	1. High input current 2. Low EMI 3. Wireless power transfer
Fig. 3 (d)	Small	Low	2L+2C	High	Common-ground	Parallel filter	Zero-voltage turn-on	1. High frequency 2. High input voltage 3. Low EMI 4. High power density

the proposed inverter and the parasitic capacitance of the switch can be absorbed by the resonant capacitor, which mitigates the effects of switching current oscillation.

Compared with Class EF topologies in [9], [13], and [19], the power output capability of the proposed Class E/F inverter is improved under parameter optimization design. Compared with the peak power output capability $C_{\mathrm{p}} = 0.1023$ for Class E resonant topologies in [15] and [18], the designed load-independent common-ground Class E/F resonant inverter can achieve higher power output capability, which verifies the advantage in the switch device selection. The actual power output capability is lower than the theoretical value for parasitic parameters and the nonlinearity of switch and passive components. Different from the series filter in [13], the value of the inductance can be reduced because the parallel filter is adopted, which further improves the system efficiency. Compared with Class E topologies and Class F/E topology in [19], the input source series with choke inductor can effectively reduce input current ripple and system electromagnetic interference in the proposed common-ground Class E/F resonant inverter.

As shown in Table IV, the proposed load-independent Class EF topologies with constant ac output characteristics are compared. Thanks to the input choke inductor, the input current ripple and system electromagnetic interference are greatly reduced for the Class EF topologies in Fig. 3(c) and (d). Generally, the loss and volume of the inductive components are greater than those of the capacitive components. Therefore, the proposed Class E/F inverter in Fig. 3(d) can achieve the lowest volume and highest power density. Obviously, turn-ON loss can be eliminated for ZVS and turn-OFF loss can be eliminated for zero-current switching. Higher power-conversion efficiency can be achieved for Class E/F resonant inverters due to the turn-ON loss exceeding the turn-OFF loss at high input voltage conditions. Likewise, the Class F/E resonant inverters are suitable for high input current condition for zero-current switching. Therefore, the choice of the Class EF topologies depends on whether turn-OFF losses or turn-OFF losses dominate.

For high-frequency switching devices such as GaN transistors, the parasitic inductor is very small. However, the parasitic capacitor is relatively large. Therefore, the Class E/F topologies with zero voltage turn-ON are more suitable for high-frequency scenarios, in which the parasitic capacitor is absorbed by a resonant capacitor. Compared with a series filter, higher quality can be achieved by the parallel filter, which improves the system efficiency and power density. However, the primary coil with a high-quality factor is used to replace the filter inductor in the series filter, which is widely applied in wireless power transfer. Moreover, the common-ground configuration is a common choice for the simple drive circuit.

From these comparisons, the proposed load-independent Class E/F topology in Fig. 3(d) is the best candidate for a high-frequency resonant inverter for most scenarios. Other Class EF topologies are suitable for specific scenarios based on their topology design and operating characteristics.

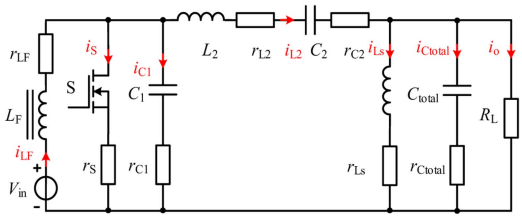

Fig. 14. Power-loss mode of the proposed load-independent common-ground Class E/F resonant inverter.

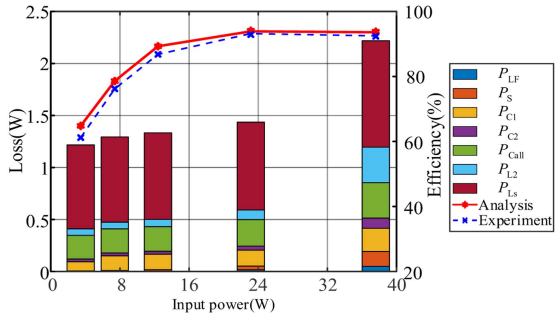

Fig. 15. Loss distribution and efficiency curves of the load-independent common-ground Class E/F resonant inverters under different input power.

C. Loss Analysis

The resonant inductors L_2 and L_s are air core inductors and the core losses are much smaller. The inductor current across L_F is almost dc so that the core losses can be ignored. The switching loss is not considered because ZVS is achieved and power loss in the gate driving circuit is not considered. Therefore, the causes of power loss are considered to be equivalent series resistances (ESRs) of the inductors and capacitors and conduction losses due to the switch ON-resistance in Fig. 14.

1) Conduction loss P_S

The conduction loss of the switch P_S is expressed as

$$P_S = r_S I_{S\_rms}^2 = \frac{r_S}{2\pi}\int_{2\pi D_{off}}^{2\pi} i_S^2(\theta)\mathrm{d}\theta. \tag{45}$$

2) Capacitor conduction losses P_{C1}, P_{C2}, and P_{Ctotal}

The conduction loss of the capacitors P_{Cr} and P_{Cs} are expressed as

$$\begin{cases} P_{C1} = r_{C1} I_{C1\_rms}^2 = \frac{r_{C1}}{2\pi}\int_0^{2\pi D_{off}} i_{C1}^2(\theta)\mathrm{d}\theta \\ P_{C2} = r_{C2} I_{L2\_rms}^2 = \frac{r_{C2}}{2\pi}\int_0^{2\pi} i_{L2}^2(\theta)\mathrm{d}\theta \\ P_{Ctotal} = r_{Ctotal} I_{Ctotal\_rms}^2 = \frac{r_{Ctotal}}{2\pi}\int_0^{2\pi} i_{Ctotal}^2(\theta)\mathrm{d}\theta \end{cases} \tag{46}$$

where r_{C1}, r_{C2}, and r_{Ctotal} are the ESRs of the capacitor C_1, C_2, and C_{total}, respectively.

3) Inductor conduction losses P_{LF}, P_{L2}, and P_{Ls}

The conduction losses of the input inductor L_F, resonant inductors L_2 and L_s are obtained as

$$\begin{cases} P_{LF} = r_{LF} I_{LF\_rms}^2 = \frac{r_{LF}}{2\pi}\int_0^{2\pi} i_{LF}^2(\theta)\mathrm{d}\theta \\ P_{L2} = r_{L2} I_{L2\_rms}^2 = \frac{r_{L2}}{2\pi}\int_0^{2\pi} i_{L2}^2(\theta)\mathrm{d}\theta \\ P_{Ls} = r_{Ls} I_{Ls\_rms}^2 = \frac{r_{Ls}}{2\pi}\int_0^{2\pi} i_{Ls}^2(\theta)\mathrm{d}\theta \end{cases} \tag{47}$$

where r_{LF}, r_{L2}, and r_{Ls} are the ESRs of the inductor L_F, L_2, and L_s, respectively.

Therefore, the inverter efficiency can be obtained as follows:

$$\eta = 1 - \frac{P_S + P_{C1} + P_{C2} + P_{Ctotal} + P_{LF} + P_{L2} + P_{Ls}}{P_{in}}. \tag{48}$$

Fig. 15 shows the loss distribution and efficiency curves of the different load-independent inverters under different input power. There is a difference in efficiency between analysis and experiment, which originated in nonlinear circuit parameters and stray losses. When the input power changes from 2 to 40 W, the peak efficiency of the designed inverter can reach 93.4%. With the input power decreasing, the system efficiency is dropped for large parasitic resistance loss in the filter inductor.

D. Load-Range Limitations

Limited by device power capabilities and circuit parasitic parameters, the following factors give the operational boundaries of the proposed inverter in practical application.

First, the ESR of the filter inductor is the main factor affecting the load-independent operation. Although ZVS can be maintained, the resonant current is large and the loss caused by ESR cannot be neglected under heavy load conditions. Consequently, the output voltage may fall below the desired value. Moreover, the power withstand capability of the device is another factor. The peak voltage and current of the switch become large in heavy load conditions, exceeding the device's withstand voltage and current values.

V. Conclusion

This article proposes a family of load-independent Class EF resonant inverters with constant ac voltage output. Moreover, the design principle and operating characteristics of load-independent Class EF resonant inverters are summarized. Furthermore, the common-ground Class E/F inverter is exemplified and its detailed load-independent analysis is provided. Without closed-loop control, the proposed common-ground Class E/F inverter can achieve ZVS and constant ac voltage output in a wide load resistance range. Additionally, the experimental results of the 21.8-W prototype verify the load-independent analysis and the peak system efficiency reaches 93.4%. However, there are still some limitations of the load-independent resonant inverter topologies, and priorities for future research are as follows.

1) The soft switching and constant ac output characteristics are lost when the load has an inductive or capacitive component. Therefore, how to achieve load-independent characteristics under resistive-inductive or resistive-capacitive load is the main research topics.
2) The circuit parameters of the resonant inverters under load-independent design are determined. Therefore, the load-independent parameter design method

to adapt to parameter changes is another research direction.

APPENDIX

To simplify the parameter design of the load-independent common-ground Class E/F resonant inverter, calculation software is developed based on MATLAB2021b. Moreover, the detailed parameter calculation process is available at https://github.com/MagicubeCheng/LoadIndependentCommonGroundClassEFParallelFilter/tree/ParameterCalculation.

REFERENCES

[1] I. A. Mashhadi, E. Ovaysi, E. Adib, and H. Farzanehfard, "A novel current-source gate driver for ultra-low-voltage applications," *IEEE Trans. Ind. Electron.*, vol. 63, no. 8, pp. 4796–4804, Aug. 2016, doi: 10.1109/TIE.2016.2554539.

[2] N. Yan, D. Dong, and R. Burgos, "A multichannel high-frequency current link based isolated auxiliary power supply for medium-voltage applications," *IEEE Trans. Power Electron.*, vol. 37, no. 1, pp. 674–686, Jan. 2022, doi: 10.1109/TPEL.2021.3102055.

[3] J. Lee, B. Bae, B. Kim, J. Lim, and B. Lee, "A load-independent battery charging system for multiple wearable devices using conductive textile," in *IEEE Trans. Ind. Electron.*, vol. 71, no. 11, pp. 15211–15215, Nov. 2024, doi: 10.1109/TIE.2024.3363752.

[4] T. Huang, Y. Chen, B. Zhang, and D. Qiu, "Shared external driver for VHF converter with a synchronous rectifier based on matching network parameters optimization," *IEEE Trans. Ind. Electron.*, vol. 71, no. 2, pp. 1481–1491, Feb. 2024, doi: 10.1109/TIE.2023.3262892.

[5] I. Nikiforidis, J. M. Arteaga, C. H. Kwan, N. Pucci, D. C. Yates, and P. D. Mitcheson, "Generalized multistage modeling and tuning algorithm for Class EF and Class ϕ inverters to eliminate iterative retuning," *IEEE Trans. Power Electron.*, vol. 37, no. 10, pp. 12877–12900, Oct. 2022, doi: 10.1109/TPEL.2022.3176391.

[6] N. Pucci, J. M. Arteaga, C. H. Kwan, D. C. Yates, and P. D. Mitcheson, "Induced voltage estimation from class EF switching harmonics in HF-IPT systems," *IEEE Trans. Power Electron.*, vol. 37, no. 4, pp. 4903–4916, Apr. 2022, doi: 10.1109/TPEL.2021.3127749.

[7] S. Aldhaher, D. C. Yates, and P. D. Mitcheson, "Modeling and analysis of Class EF and Class E/F inverters with series-tuned resonant networks," *IEEE Trans. Power Electron.*, vol. 31, no. 5, pp. 3415–3430, May 2016, doi: 10.1109/TPEL.2015.2460997.

[8] C. Liu, Y. Guan, J. Liu, Y. Wang, and D. Xu, "Seamless control strategy and hybrid module architecture of wide power range inverter," *IEEE Trans. Ind. Inform.*, vol. 19, no. 8, pp. 8575–8587, Aug. 2023, doi: 10.1109/TII.2022.3220861.

[9] L. Roslaniec, A. S. Jurkov, A. A. Bastami, and D. J. Perreault, "Design of single-switch inverters for variable resistance/load modulation operation," *IEEE Trans. Power Electron.*, vol. 30, no. 6, pp. 3200–3214, Jun. 2015, doi: 10.1109/TPEL.2014.2331494.

[10] R. E. Zulinski and K. J. Grady, "Load-independent class E power inverters. I. theoretical development," *IEEE Trans. Circuits Syst.*, vol. 37, no. 8, pp. 1010–1018, Aug. 1990, doi: 10.1109/31.56074.

[11] M. Mizutani, S. Koyama, S. Abe, and T. Ohira, "Geodesic theory of zero-voltage-switching RF power inverters for constant-voltage or -current output operation," in *Proc. IEEE Int. Conf. Power Energy*, 2020, pp. 83–88, doi: 10.1109/PECon48942.2020.9314539.

[12] J. M. Rivas, Y. Han, O. Leitermann, A. D. Sagneri, and D. J. Perreault, "A high-frequency resonant inverter topology with low-voltage stress," *IEEE Trans. Power Electron.*, vol. 23, no. 4, pp. 1759–1771, Jul. 2008, doi: 10.1109/TPEL.2008.924616.

[13] S. Aldhaher, D. C. Yates, and P. D. Mitcheson, "Load-independent Class E/EF inverters and rectifiers for MHz-switching applications," *IEEE Trans. Power Electron.*, vol. 33, no. 10, pp. 8270–8287, Oct. 2018, doi: 10.1109/TPEL.2018.2813760.

[14] T. Sensui and H. Koizumi, "Load-independent Class E zero-voltage-switching parallel resonant inverter," *IEEE Trans. Power Electron.*, vol. 36, no. 11, pp. 12805–12818, Nov. 2021, doi: 10.1109/TPEL.2021.3077077.

[15] L. Zhang and K. Ngo, "A constant-current ZVS Class-E inverter with finite input inductance," *IEEE Trans. Ind. Electron.*, vol. 68, no. 8, pp. 7693–7696, Aug. 2021, doi: 10.1109/TIE.2020.2998764.

[16] K. Shinde and H. Koizumi, "Capacitive power transfer system using a load-independent class E zero voltage switching parallel resonant inverter and a class D voltage-driven rectifier," *IEEE Trans. Circuits Syst. II, Exp. Briefs*, vol. 71, no. 9, pp. 4366–4370, Sep. 2024, doi: 10.1109/TCSII.2024.3384299.

[17] A. Komanaka, W. Zhu, X. Wei, K. Nguyen, and H. Sekiya, "Generalized analysis of load-independent ZCS parallel-resonant inverter," *IEEE Trans. Ind. Electron.*, vol. 69, no. 1, pp. 347–356, Jan. 2022, doi: 10.1109/TIE.2021.3053888.

[18] Y. Cheng, Y. Guan, T. Yao, Y. Wang, W. Wang, and D. Xu, "Topology construction strategy of load-independent single-switch resonant inverter," *IEEE Trans. Ind. Electron.*, vol. 71, no. 9, pp. 10580–10590, Sep. 2024, doi: 10.1109/TIE.2023.3342309.

[19] W. Zhu, Y. Komiyama, A. Komanaka, K. Nguyen, and H. Sekiya, "Analysis of load-independent ZCS parallel-resonant inverter with constant current," *IEEE Trans. Ind. Electron.*, vol. 71, no. 9, pp. 10433–10443, Sep. 2024, doi: 10.1109/TIE.2023.3333019.

[20] Y. Komiyama, A. Komanaka, W. Zhu, A. Konishi, K. Nguyen, and H. Sekiya, "Analysis and design of load-independent series resonant power amplifier with constant current output and its application for WPT system," *IEEE Trans. Power Electron.*, vol. 39, no. 5, pp. 6515–6525, May 2024, doi: 10.1109/TPEL.2024.3367373.

[21] X. Huang, Y. Lin, Y. Dou, S. Lin, and J. Huang, "Load-independent push–pull class-Φ_2 inverter with single compact three-winding inductor," *IEEE Trans. Power Electron.*, vol. 38, no. 10, pp. 11916–11927, Oct. 2023, doi: 10.1109/TPEL.2023.3298254.

Yi Cheng (Student Member, IEEE) was born in Anhui Province, China, in 1999. He received the B.S. and M.S. degrees in electrical engineering in 2021 and 2023, respectively, from the Harbin Institute of Technology, Harbin, China, where he is currently working toward the Ph.D. degree in electrical engineering.

His research interests include high-frequency and very high-frequency resonant inverters.

Yueshi Guan (Senior Member, IEEE) was born in Heilongjiang Province, China, in 1990. He received the B.S., M.S., and Ph.D. degrees in electrical engineering from the Harbin Institute of Technology (HIT), Harbin, China, in 2013, 2015, and 2019, respectively.

Since 2024, he has been a Professor with the Department of Electrical and Electronics Engineering, HIT. His research interests include high-frequency and very high-frequency converters, single-stage ac–dc converters, and high-conversion ratio converters.

Tingting Yao (Member, IEEE) received the B.S., M.S., and Ph.D. degrees in electrical engineering from the Harbin Institute of Technology, Harbin, China, in 2013, 2015, and 2023, respectively.

She is currently an Associate Professor with the College of Computer and Control Engineering, Northeast Forestry University, Harbin. Her research interests include the areas of high conversion ratio converters and high-frequency resonant converters.

Jiachao Zong (Student Member, IEEE) was born in Anhui Province, China, in 2001. He received the B.S. degree in electrical engineering in 2023 from the Harbin Institute of Technology, Harbin, China, where he is currently working toward the M.S. degree in electrical engineering.

His research interests include MHz wireless power transfer, simultaneous wireless power and data transmission, and electromagnetic compatibility.

Yijie Wang (Senior Member, IEEE) was born in Heilongjiang Province, China, in 1982. He received the B.S., M.S., and Ph.D. degrees in electrical engineering from the Harbin Institute of Technology, Harbin, China, in 2005, 2007, and 2012, respectively.

From 2012 to 2014, he was a Lecturer with the Department of Electrical and Electronics Engineering, Harbin Institute of Technology. From 2014 to 2017, he was an Associate Professor. Since 2017, he has been a Professor with the Department of Electrical and Electronics Engineering, Harbin Institute of Technology. His research interests include wireless power transfer (WPT), dc–dc converters, soft-switching power converters, power factor correction circuits, digital control electronic ballasts, and LED lighting systems

Dr. Wang is an Associate Editor for IEEE TRANSACTIONS ON INDUSTRIAL ELECTRONICS, IEEE JOURNAL OF EMERGING AND SELECTED TOPICS IN POWER ELECTRONICS, IEEE ACCESS, *IET Power Electronics*, and *Journal of Power Electronics*.

Dianguo Xu (Fellow, IEEE) was born in Heilongjiang, China, in 1960. He received the B.S. degree in control engineering from Harbin Engineering University, Harbin, China, in 1982, and the M.S. and Ph.D. degrees in electrical engineering from the Harbin Institute of Technology (HIT), Harbin, China, in 1984 and 1989, respectively.

In 1984, he joined the Department of Electrical Engineering, HIT, as an Assistant Professor. Since 1994, he has been a Professor with the Department of Electrical Engineering, HIT. From 2000 to 2010, he was the Dean of the School of Electrical Engineering and Automation, HIT. He is the Vice President of HIT. He authored or coauthored more than 600 technical papers. His research interests include renewable energy generation technology, power quality mitigation, sensorless vector-controlled motor drives, and high-performance servo systems.

Dr. Xu is currently an Associate Editor for IEEE TRANSACTIONS ON INDUSTRIAL ELECTRONICS, IEEE TRANSACTIONS ON POWER ELECTRONICS, and IEEE JOURNAL OF EMERGING AND SELECTED TOPICS IN POWER ELECTRONICS. He is the Chairman of the IEEE Harbin Section. He was the recipient of the 2018 IEEE IAS Outstanding Achievement Award.